UNIVERSITY OF CRETE – DEPARTMENT OF PHYSICS

INSTITUTE OF ELECTRONIC STRUCTURE AND LASER-FOUNDATION FOR RESEARCH AND TECHNOLOGY

Diploma Thesis

Metamaterial Perfect Absorbers in THz and Optical regime

By

Manolis Petrakakis

Supervisor: Prof. Maria Kafesaki
Academic advisor: Prof. George Tsironis

October 2014

Dedicated to my Father and Mother,

Nikos and Sofia.

"Reach what you cannot"
Nikos Kazantzakis, *Report to Greco*

ABSTRACT

In this work, we study the electromagnetic response of the Metamaterial Perfect Absorbers. In the first part, we present the underlining theoretical background of Metamaterial Perfect Absorbers. Three different approaches are introduced: the 'Pedrian' approach, interference theory and Single resonant Metamaterial Surfaces approach. In the second part, we examine the electromagnetic response of a specific structure that has taken lot of attention due to the remarkable applications for many different devices such as photovoltaics. In particular, we study different geometries of 2-D and 3-D composite media with specific optical constants in order to design a near-unity metamaterial absorber (i.e. a structure which captures all incident radiation).

ACKNOWLEDGMENTS

My deepest respect is for my thesis advisors, Prof. Maria Kafesaki and Prof. Eleftherios Economou . Their guidance, support and patience were crucial to succeed this work.

My sincere appreciation goes to Dr. George Kenenakis and Dr. Anna Tasolamprou for their encouragement and willingness to always answer my questions.

Furthermore, I would like to thank Prof. Costas Soukoulis, Prof. Nikos Katsarakis and Dr. Sotiris Droulias for their helpful advice at the weekly group meetings.

I am also grateful for the opportunity to work in Photonic-, Phononic- and Meta-Materials (PPM) group.

Finally, I would like to thank the Foundation of Research and Technology – Hellas (FO.R.T.H.) for the financial support during my last year of studies.

TABLE OF CONTENTS

PART I - THEORETICAL BACKGROUND

CHAPTER 1

1 Metamaterial Perfect Absorbers

1.1 Introduction

The first part of this work would include the necessary theoretical background for Metamaterial Perfect Absorbers. The demonstration of Metamaterial perfect absorbers [1,2] represents one of the most important applications employing the astonishing properties found in Metamaterial [3-5]. We will present three different perspectives to have a complete overview of the phenomena that occur in Metamaterial perfect absorbers: (a) the standard theoretical approach [2,6] (b) interference theory [7] and (c) single-resonance model based on Metamaterial surfaces [8].

1.2 Standard Theoretical approach

The original idea [2] is that, in Metamaterial with simultaneous electrical and magnetic resonances, both of the effective permittivity $\varepsilon_{eff}(\omega)$ and permeability $\mu_{eff}(\omega)$ are highly dispersive and can be tailored independently. At certain frequencies the effective impedance, which is defined as $z(\omega) = \sqrt{\frac{\mu_{eff}(\omega)}{\varepsilon_{eff}(\omega)}}$, matches to the free space impedance Z_0, and therefore the reflection is minimized. If at the same frequency the Metamaterial is also of high loss, which causes very low transmission, then near-unity absorption can occur within an ultra-thin layer of material. Under such considerations, in a typical Metamaterial absorber, the magnetic resonance from the bi-layered metal structure [9, 10] is essential, and each layer of metal structure also provides the electrical response. As a direct evidence of the magnetic resonance in Metamaterial absorbers, the surface currents excited in the two metal layers are found to be anti-parallel [11].

1.3 Analytical relations for Transmission and Reflection

The absorptivity *A(ω)* of a material is given by the transmission *T(ω)* and reflectance *R(ω)* as *A(ω)=1-T(ω)-R(ω)*. In terms of the complex transmissivity ($\tilde{t}$) and reflectivity ($\tilde{r}$), this can be written as $A=1-|\tilde{t}(\omega)|^2-|\tilde{r}(\omega)|^2$. Therefore, *A=1* when *T=R=0*. In Ref. 12, the frequency-dependent transmissivity $\tilde{t}(\omega)$ was determined to be dependent on the complex index of refraction $\tilde{n}(\omega) = n_1 + in_2$ and impedance $\tilde{Z}(\omega) = Z_1 + iZ_2$ for a slab of length d as

$$t(\omega)^{-1} = \left[cos(\tilde{n}kd) - \frac{i}{2}\left(\tilde{z} + \frac{1}{\tilde{z}}\right) sin(\tilde{n}kd)\right] e^{ikd}\,, \tag{1}$$

where $k=\omega/c$ and c is the speed of light in the vacuum. We use the convention where a subscripted 1 and 2 denote the real and imaginary parts of a complex function, respectively. As $\tilde{Z}$ approaches unity (the free space value), the reflectivity will drop to zero and the transmissivity will be determined entirely by $\tilde{n}$ as follows:

$$t^{-1} = [cos(\tilde{n}kd) - isin(\tilde{n}kd)]e^{ikd}\,, \tag{2}$$

Upon substitution of the exponential forms this becomes

$$t^{-1} = e^{-i(n_1-1)kd}e^{n_2kd} \tag{3}$$

So the transmission is ($T = |\tilde{t}|^2$) is

$$T=e^{-2n_2kd} \tag{4}$$

Therefore, as n_2 approaches infinity for a given d,

$$lim_{n_2\to\infty}\, T = 0\,. \tag{5}$$

The combined dielectric and magnetic losses in the systemare characterized by n_2. Therefore the physical interpretation of the above

derivation is that in the absence of reflectionsthe transmission of an electromagnetic wave with a wavevector k through a slab of thickness d is determined entirely by losses in the slab. To create a very high absorber it is then necessary for $\tilde{Z} = 1$ at a point where n_2 is large. The higher the value of n_2 that can be obtained, the thinner the slab can be in the propagation direction. In this manner, one can overcome the quarter-wavelength thickness requirement of traditional Salisbury screens and Jaumann absorbers[13,14].

Precise control of $\tilde{n}$ and $\tilde{Z}$ is necessary to realize a high absorber. Electromagnetic Metamaterials are prime candidates for this task since they can be designed to couple to electric and magnetic components of light. This enables precise tuning of the complex frequency-dependent permittivity $\tilde{\varepsilon}(\omega)$ and permeability $\tilde{\mu}(\omega)$ of a metamaterial slab. The index of refraction $\tilde{n}$ and impedance $\tilde{Z}$ are in turn given by

$$\tilde{n} = \sqrt{\tilde{\varepsilon}(\omega)\tilde{\mu}(\omega)} \quad \text{and} \quad \tilde{Z} = \sqrt{\frac{\tilde{\mu}(\omega)}{\tilde{\varepsilon}(\omega)}}$$

Metamaterials are typically highly resonant in $\tilde{\varepsilon}(\omega)$ and/or $\tilde{\mu}(\omega)$, where the relevant optical constants approximate the form of a complex oscillator in frequency,

$$\varepsilon(\omega), \mu(\omega) = \varepsilon_\infty, \mu_\infty + \frac{F_{\varepsilon,\mu}\omega^2}{\omega_{0\varepsilon,\mu}^2 - \omega^2 - i\gamma\omega} \ , \qquad (6)$$

where F is the oscillator strength, γ is the damping, ω_0 is the center frequency of the oscillator, and $\varepsilon_\infty, \mu_\infty$ are high frequency contributions to ε and μ .

This form for an oscillator describes the frequency response of metamaterials and we term this a "Pendrian" after Ref. 15.

We consider a single-frequency operation point, defined by ω_0, for two oscillators with identical frequency dependence such that $\tilde{\varepsilon}(\omega) = \tilde{\mu}(\omega)$; then $\tilde{Z}(\omega_o) = 1$ and $n_2(\omega_o)$ is maximized with a value of

$$n_2(\omega_0) = \frac{F\omega_0}{\gamma} \tag{7}$$

which, according to Eq. (4), yields

$$A(\omega_0) = 1 - e^{2\left(\frac{F\omega_0^2 d}{c\gamma}\right)}. \tag{8}$$

For the more realistic case, when $\varepsilon_\infty \neq \mu_\infty$ then $\tilde{Z}(\omega_o) \neq 1$ and A is no longer determined solely by n_2. However, for large n_2, $T(\omega_o)$ remains low and $R(\omega_o)$ can be written approximately in terms of $Z(\omega)$ (Ref. 12) such that

$$R(\omega_0) = \left(\frac{Z(\omega_0)-1}{Z(\omega_0)+1}\right)^2. \tag{9}$$

Regardless of ε_∞ and μ_∞ an optimal narrow-band absorber must maximize F with respect to γ in both ε and μ. F is determined by the geometry, filling factor, and conductivity of the two metallizations. γ is determined by losses in the metallization and substrate. The optimal absorber will then use the MM geometries with the maximum possible filling factor. Furthermore, metallization and substrate should be chosen to minimize losses at the operation frequency as determined by Eq. (7) above.

1.4 Interference Theory

The perfect absorption [2] on metamaterial absorbers was qualitatively attributed to matching the impedance $z = \sqrt{\frac{\mu_{eff}}{\varepsilon_{eff}}}$ of the bulk metamaterial to that of vacuum where μ_{eff} and ε_{eff} are the bulk effective magnetic permeability and bulk effective electric permittivity of the metamaterial, respectively. While all of the above arguments seem to be plausible and accepted by a majority of researchers [16-18], fundamental questions remain. In fact, such a metamaterial absorber can be equivalent to a single layer of atoms (or molecules), and it is strongly inhomogeneous in the wave propagating direction [12]. So it can hardly be considered as an effective bulk medium where the constitutive parameters ε(ω) and μ(ω) apply. Instead, the metamaterial perfect absorbers have been described more meaningfully by several different models such as *interference models* [7]. Without loss of generality we present a typical cross-resonator system (Metal-Dielectric Spacer-Metal). We choose to present only the results. As shown in the inset to Fig. 1, at the air-spacer interface with cross-resonator array, the incident light is partially reflected back to air with a reflection coefficient $\tilde{r}_{12}=r_{12}e^{i\varphi_{12}}$.

And partially transmitted into the spacer with a transmission coefficient $\tilde{t}_{12}=t_{12}e^{i\theta_{12}}$.

The latter continues to propagate until it reaches the ground plane, with a complex propagation phase $\tilde{\beta} = \beta_r + i\beta_i = \sqrt{\tilde{\varepsilon}_{spacer}}k_o d$ where k_o is the free space wavenumber, βr is the propagation phase, and βi represents the absorption in the spacer. After the reflection at the ground plane and addition of another propagation phase$\tilde{\beta}$, partial reflection and transmission occur again at the air-spacer interface with cross-resonators with coefficients $\tilde{r}_{21} = r_{21}e^{i\varphi_{21}}$ and $\tilde{t}_{21} = t_{21}e^{i\varphi_{21}}$.

Similar to the light propagation in a stratified media [19], the overall reflection is then the superposition of the multiple reflections:

$$\tilde{r} = \tilde{r}_{12} - \frac{\tilde{t}_{12}\tilde{t}_{21}e^{i2\tilde{\beta}}}{1+\tilde{r}_{21}e^{i2\tilde{\beta}}} \tag{10}$$

where the first term is the reflection directly from the cross-resonator array, and the second term, including the "−" sign, is the reflection resulting from superposition of the multiple reflections between the cross-resonator array and ground plane. The absorptance is then retrieved through $A=1-|\tilde{r}(\omega)|^2$ since the transmission is zero.

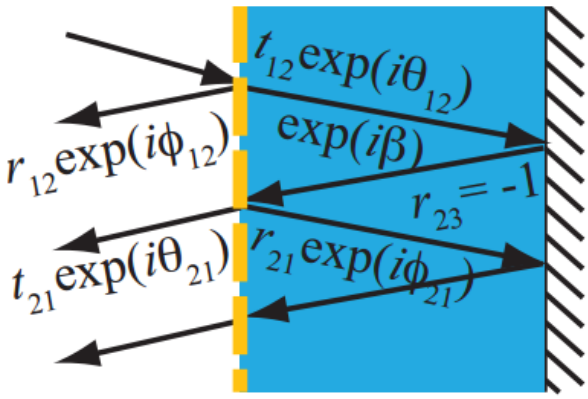

Figure 1. The interference within the spacer

The physical explanation of a metamaterial absorber is then as follows. The multiple reflections in the metamaterial absorber, i.e. the second term in Eq. (10), constructively interfere as evidenced by the fact that near 1 THz the phase change of a round trip is $2\beta r + \varphi_{21} + 180^{\circ} \approx 360^{\circ}$. The superposition of the multiple reflections then destructively interferes with the direct reflection from the air-spacer interface with cross-resonators, i.e. the first term in Eq. (10). With an optimized spacer thickness and in a narrow frequency range, these two terms completely cancel each other out resulting in zero reflection.

For other spacer thicknesses or frequencies the amplitude and phase do not match and these two terms only partially cancel out or may even constructively add each other, resulting in: i) a reduced absorption peak and ii) corresponding frequency shift of the absorption peak when the spacer thickness deviates from the optimized value, and iii) dramatically reduced absorption when the frequency goes away from the center frequency. Obviously, this explanation does not involve any near-field interaction or magnetic resonance between the two metal layers in the metamaterial absorber. That is, the resonator array and ground plane in the 'coupled' metamaterial absorber system can be indeed decoupled (fig2).

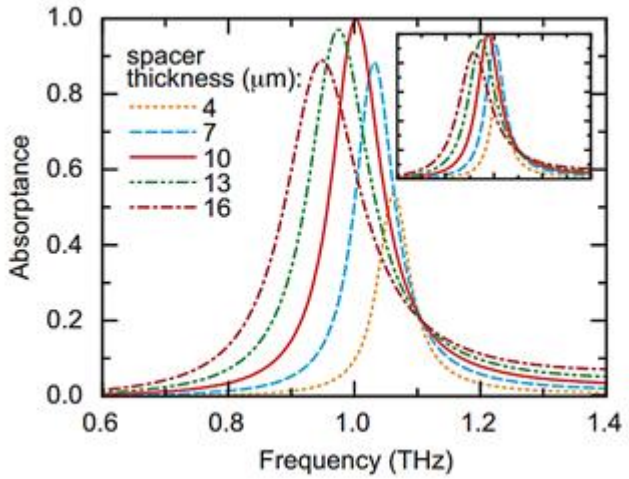

Figure 2. Calculated absorptance in the decoupled Metamaterial absorber using the interference model for various spacer thicknesses.

We have shown that it is *not* required in a metamaterial absorber to have simultaneous electric and magnetic responses, which has previously been considered as the foundation of metamaterial absorbers. It is the destructive interference between the direct reflection and the following multiple reflections that effectively traps light in the metamaterial absorbers and eventually causes the high absorption.

1.5 Metamaterial Surfaces – Single Resonance Model

In this approach we show that the surface impedance z of a broad-band Metamaterial absorber (BBMA) can be obtained from impedances z_i of the constitutive narrow-band Metamaterial absorbers (NBMA) using a simple addictive formula which is valid as long as the SPP's propagation lengths are much smaller than the separation of the NBMAs. We start by introducing a simple single-resonance model of an NNBA based on a periodic structure shown in (fig3). The structure coupled to the incident radiation is described within the framework of a single resonator model [20]. An open resonator model is described by its natural frequency, $\omega_{o,}$ and finite lifetimes, $\tau_o=1/\omega_{io}$ and $\tau_e=1/\omega_{ie}$, respectively determined by the Ohmic and radiative losses. The interaction between the resonator and the incident field of amplitude E_I is described by the following equations:

$$\frac{d}{dt}a = -i\omega_0\, a - (\omega_{i0} + \omega_{ie})a + \sqrt{2\omega_{ie}}$$

$$E_R = -E_I + \sqrt{2\omega_{ie}}\; a, \qquad (11)$$

where α and E_R are the amplitudes if the resonator and the reflected field , respectively. The specific geometry of the resonator that includes the ground plane is manifested in the expression for $E_{R,}$ which is a superposition of the resonator and ground plane reflection. Within this simple single-resonance model, the surface impedance defined as $z=(1+r)/(1-r)$ where $r= E_R/ E_I$, is given by :

$$z = \frac{\omega_{ie}}{-i(\omega-\omega_o)+\omega_{io}} \qquad (12)$$

and all optical parameters of NBMA are determined by three parameters ω_o , ω_{ie} , ω_{io} .

By tuning the geometric parameters of the NBMA one can engineer this three parameters and achieve $z=1$ (and, therefore perfect absorption) whenever the critical coupling condition $\omega_{ie} = \omega_{io}$ is satisfied.

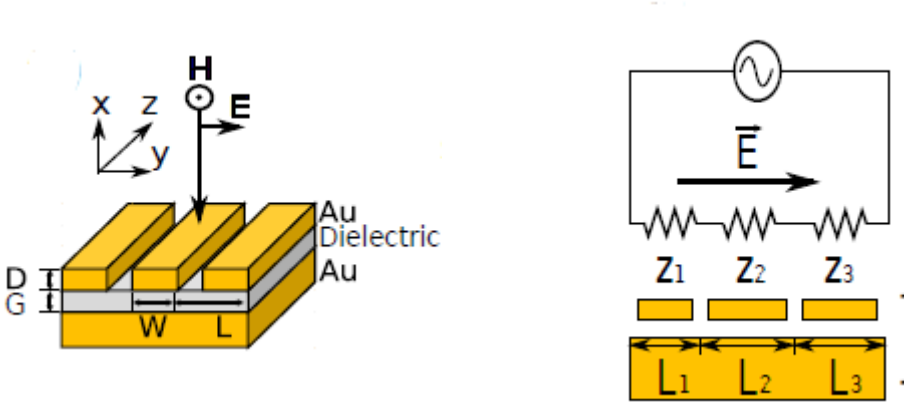

Figure 3. Schematic of the Narrow-Band Metamaterial Absorber (left). Illustration of the circuit model (right).

Two important features of NBMAs described in Fig.3 make them promising building blocks for designing a BBMA. First, their period is strongly sub-wavelength: $L_i \ll \lambda^{(i)} = 2\pi c/\omega_o^{(i)}$.

That implies that a sub-wavelength unit cell $L = \sum_i L_i \leq \lambda$ of a BBMA can accommodate a large number of NBMA-based sub-units satisfying $L_i \ll L \leq \lambda$. Second, the propagation length $\lambda_{spp}^{(i)} < L^i$ .This property has been shown [21] to be related to the wide angle absorbance of NBMA.

We have demonstrated that a broad-band metamaterial absorber (BBMA) can be designed by constructing a super-lattice absorbing at different frequencies. Based on a single oscillator model and a series circuit model, broadband absorbers with multiple perfectly absorbing peaks are shown to be attainable

References

[1] A. Al`u, F. Bilotti, N. Engheta, and L. Vegni, "A thin absorbing screen using Metamaterial complementary pairs," *in Proceedings of the International Conference on Electromagnetics in Advanced Applications*, (Turin, Italy, September 12-16, 2005), pp. 75‑78.

[2] N. I. Landy, S. Sajuyigbe, J. J. Mock, D. R. Smith, and W. J. Padilla, 'Perfect Metamaterial absorber' Phys. Rev.Lett. **100**, 207402 (2008).

[3] D. R. Smith, W. J. Padilla, D. C. Vier, S. C. Nemat-Nasser, and S. Schultz 'Composite Medium with Simultaneously Negative Permeability and Permittivity' Phys. Rev. Lett. **84**, 4184‑4187 (2000).

[4] H.-T. Chen, J. F. O' Hara, A. K. Azad, and A. J. Taylor, "Manipulation of terahertz radiation using metamaterials," Laser Photon. Rev. **5**, 513‑533 (2011).

[5] W. Cai and V. Shalaev, *Optical Metamaterials: Fundamentals and Applications* (Springer, 2010).

[6] PhysRevB.**79**. 10.1103/125104 N. I. Landy, C. M. Bingham, T. Tyler, N. Jokerst, D. R. Smith, and W. J. Padilla.

[7] 10.1364/OE.20.007165, Optics Express, Vol. **20**, Issue 7, pp. 7165-7172 (2012), Hou-Tong Chen.

[8] 10.1364/OL.37.000308**,**Optics Letters, Vol. **37**, Issue 3, pp. 308-310 (2012), Chihhui Wu and Gennady Shvets.

[9] S. Zhang, W. Fan, N. C. Panoiu, K. J. Malloy, R. M. Osgood, and S. R. J. Brueck, "Experimental demonstration of near-infrared negative-index metamaterials," Phys. Rev. Lett. **95**, 137404 (2005).

[10] V. M. Shalaev, W. Cai, U. K. Chettiar, H.-K. Yuan, A. K. Sarychev, V. P. Drachev, and A. V. Kildishev, "Negative index of refraction in optical metamaterials," Opt. Lett. **30**, 3356–3358 (2005).

[11] H. Tao, N. I. Landy, C. M. Bingham, X. Zhang, R. D. Averitt, and W. J. Padilla, "A metamaterial absorber for the terahertz regime: Design, fabrication and characterization," Opt. Express **16**, 7181-7188 (2008).

[12] D. R. Smith, D. C. Vier, T. Koschny, and C. M. Soukoulis, Phys.Rev. E **71**, 036617 (2005).

[13] H. Tao, N. I. Landy, C. M. Bingham, X. Zhan, R. D. Averitt, and W. J. Padilla, Opt. Express **16**, 7181 (2008).

[14] A. J. Gatesman, A. Danylov, T. M. Goyette, J. C. Dickinson, R.H. Giles, W. Goodhue, J. Waldman, W. E. Nixon, and W. Hoen,Proc. SPIE 6212, 62120E (2006).

[15] J. B. Pendry, A. J. Holden, D. J. Robbins, and W. J. Stewart, IEEE Trans. Microwave Theory Tech. **47**, 2075 (1999).

[16] Y. Avitzour, Y. A. Urzhumov, and G. Shvets, "Wide-angle infrared absorber based on a negative-index plasmonic metamaterial," Phys. Rev. B **79**, 045131 (2009).

[17] N. Liu, M. Mesch, T. Weiss, M. Hentschel, and H. Giessen, "Infrared perfect absorber and its application as plasmonic sensor," Nano Lett. **10**, 2342-2348 (2010).

[18] J. Hao, L. Zhou, and M. Qiu, "Nearly total absorption of light and heat generation by plasmonic metamaterials," Phys. Rev. B **83**, 165107 (2011).

[19] M. Born and E. Wolf, '*Principles of optics'* (Pergamon, 1980), 6th ed.

[20] Hermann A.Haus, '*Waves and fields in optoelectronics'* (Prentice-Hall,1984)

[21] 'Large-area wide-angle spectrally selective plasmonic absorber' Phys. Rev. B **84**, 075102(2011) Chihhui Wu, Burton Neuner, III, Gennady Shvets, Jeremy John, Andrew Milder, Byron Zollars, and Steve Savoy

CHAPTER 2

2 Finite Element Methods in Electromagnetics

2.1 Introduction

The goal of Finite Element Method is to discretize the domain of a differential equation problem which has *infinite* degrees of freedom, to produce a discrete problem, which has *finite* degrees of freedom and therefore can be solved via computer. The underlining variational principle is briefly presented.

2.2 The Finite Element Analysis

The main idea behind the method is the representation of the computational domain Ω with smaller subdomains Ω^e (e=1, 2, 3…, M) called 'finite *elements'*. The process is called meshing. For 1-D domain (a straight or curved line) the elements are short line segments such as to form approximately the original line (fig.1*)*. In a 3-D solution, the domain may be subdivided into tetrahedral, triangular prisms, or rectangular bricks. The type and accuracy are selected carefully in order to spend less computational time but succeed convergence. In a modal problem, the unknown quantity *(e.g. electric potential)* inside an element is interpolated based on the values at the nodes. The accuracy of the solution depends on the order of these polynomials, which may be linear, quadratic, or higher order. The solution is obtained after solving a system of linear equations. To form such a linear system of equations, the differential equation and the associated boundary conditions must first be converted to an integro-differential formulation by minimizing a functional.

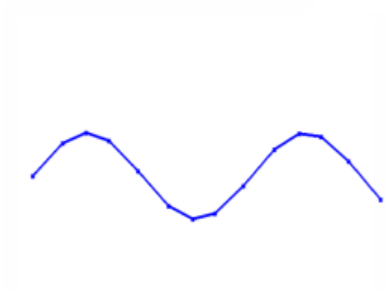

Figure1. Linemeshing of sinusoidal string into short line parts.

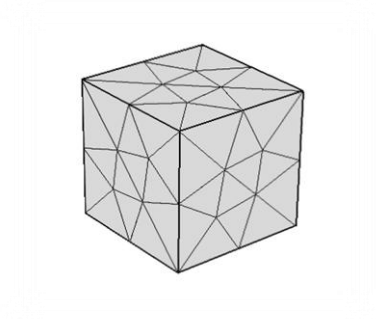

Figure 2. Triangular Meshing of a 3-D bulk box .

2.3 Variational Principle

In this chapter we follow the basic steps of the method to treat a general one-dimensional boundary-value problem. We note that numerical methods are sheldomly used in one-dimensional electromagnetic problems since few of these problems result in a model complicated enough to require numerical solution. Nevertheless, because of its simplicity, the one-dimensional problem is ideal for demonstrating formulation of the finite element method.

The boundary-value problem to be considered is defined by the differential equation:

$$-\frac{d}{dx}\left(a\frac{d\Phi}{dx}\right)+\beta\Phi=f \qquad x\epsilon(0,L) \qquad (2.2.1)$$

Where Φ *is the potential*, α and β are known parameters associated with the physical properties of the solution domain, and *f* is a known excitation function or source. The standard one- dimensional Laplace, Poisson, and Helmholtz equations are special forms of (2.2.1)

$$[\Phi(x)]_{x=0}=p \qquad (2.2.2)$$

and

$$\left[a\frac{d\Phi}{dx}+\gamma\Phi\right]_{X=L}=q \qquad (2.2.3)$$

Where p, γ and q are known parameters or functions. In the above (2.2.2) is usually referred to as a boundary condition of the first kind or Dirichlet condition, whereas (2.2.3) is referred to as a boundary condition of third kind.

A boundary condition of the second kind, or Neumann condition is a special form of (2.2.3) with γ=0. The reason we choose to apply two different boundary conditions at the two endpoints of the domain is simply to demonstrate their different treatment and to maintain the generality of our analysis.

If inside the domain at some points there are discontinuities or abrupt changes, say at $x_d (0 < x_d < L)$, the function Φ is to satisfy the continuity conditions

$$\Phi_{x=x_d+0} = \Phi_{x=x_d-0}$$

and

$$\left[a\frac{d\Phi}{dx}\right]_{x=x_d+0} = \left[a\frac{d\Phi}{dx}\right]_{x=x_d-0}$$

Where $x = x_d + 0$ indicates that x approaches x_d from the right-hand side and $x = x_d - 0$ indicates that x approaches x_d from the left-hand side.

To use the variational method to formulate finite element equations , we need first to establish the require variational principle. For the problem defined above , it can be shown that its solution can be obtained by solving the equivalent variational problem defined by

$$\begin{cases} \delta F(\Phi) = 0 \\ \Phi|_{x=0} = p \end{cases} \qquad (2.2.6)$$

Where

$$F(\Phi) = \frac{1}{2}\int_0^L \left[a\left(\frac{d\Phi}{d\chi}\right)^2 + \beta\Phi^2\right]dx - \int_0^L f\Phi\, dx + \left[\frac{\gamma}{2}\Phi^2 - q\Phi\right]_{\chi=L} . \quad (2.2.7)$$

The implication of (2.2.6) is that we seek the stationery point of the functional *F(Φ)* under the given Dirichlet boundary condition. We note that for convenienience we have used Φ instead $\widetilde{\Phi}$ in the functional above. It is understood, hovewever, that whenever Φ appears in a functional or in weighted

residual equation, we consider it a trial function or an approximate solution rather than the exact solution.

To prove that the variational formulation stated above is equavalent to the boundary-value problem defined in (2.2.1)-(2.2.3), let us take first variation of F(Φ) with respect to Φ

$$\delta F(\Phi) = \int_0^L \left[a\left(\frac{d\Phi}{dx}\right)\left(\frac{d\delta\Phi}{dx}\right) + \beta\Phi\delta\Phi \right] dx + [\gamma(\Phi - q)\delta\Phi]_{x=L} - \int_0^L f\delta\Phi \, dx \quad . (2.2.8)$$

Assuming at present that α is continuous in the entire domain, (2.2.8) can be written as

$$\delta F(\Phi) = \int_0^L \left[-\frac{d}{dx}\left(a\frac{d\Phi}{dx}\right) + \beta\Phi \right] \delta\Phi dx \quad + \quad \left[a\frac{d\Phi}{dx}\delta\Phi \right]_{x=0}^{x=L} + \quad [(\gamma\Phi - q)\delta\Phi]_{x=L} - \int_0^L f\delta\Phi \, dx. \qquad (2.2.9)$$

by intergrating the first term on the right-hand side by parts.Since Φ has a fixed value at *x=0, δΦ(x=0)=0.* As a result ,

$$\delta F(\Phi) = \int_0^L \left[-\frac{d}{dx}\left(a\frac{d\Phi}{dx}\right) + \beta\Phi \right] \delta\Phi dx \quad + \quad \left[(a\frac{d\Phi}{dx} + \gamma\Phi - q)\delta\Phi \right]_{x=L} - \int_0^L f\delta\Phi \, dx. \quad (2.2.10)$$

Imposing the stationary requirement δF=0 and because $\delta\Phi$ is an arbitary variation , this implies that both integral and boundary terms must vanish .Thus,

$$-\frac{d}{dx}\left(a\frac{d\Phi}{dx}\right) + \beta\Phi - f = 0 \quad (2.2.12)$$

$$a\frac{d\Phi}{dx} + \gamma\Phi - q = 0 \quad (2.2.13)$$

Comparing (2.2.12) and (2.2.13) with (2.2.1) and (2.2.2), we conclude that inded the solution to the variational problem (2.2.6) is also the solution to the boundary-value problem defined by (2.2.1) (2.2.3). Equation (2.2.12) is called the Euler equation of the functional F(Φ) given in (2.2.7)[2].

Therefore, the finite element method has its origins to a simple minimization of a functional. Such as a physical system has to minimize energy in order to be stable, the Finite Element Analysis finds the best fitted functional and minimizes it to return a stable solution.

References

[1] ‘Introduction to the Finite Element Method in Electromagnetics’, Anastasis Polycarpou, Constantine Balanis, Morgan & Claypool 2006.

[2] ‘The Finite Element Method in Electromagnetics’, Jianming Jin, John Wiley & Sons, 2002.

PART II – COMPUTATIONAL PART

CHAPTER 3

3 Metamaterial Perfect Absorber in THz and optical regime

3.1 Introduction

In this part we suggest a 2-dimensional Metamaterial periodic unit cell that is a perfect candidate to achieve a near-unity absorbance. The result is attributed to the geometry and the optical constants. We use the Finite-Element-based program COMSOL Multiphysics [1].

3.2 Geometry of the Metamaterial structure

The structure that we are interested in is infinitely long in the x-direction [2]. It consists of a three-layer Metal-Semiconductor-Metal (MSM) system. The back plate metal is tungsten (yellow) and has a height 0.2μm. On top of tungsten back plate is a spacer semiconductor layer made out of Silicon Nitride (SiN) depicted in blue. It's height is h and would be our free parameter to accomplish unity absorbance. On top of the spacer layer are metallic wires (or stripes) with a rectangular cross-section. Their arrangement is described by a *lattice constant* $\alpha=2\mu m$. To save computational time we have the following unit cell (fig.1):

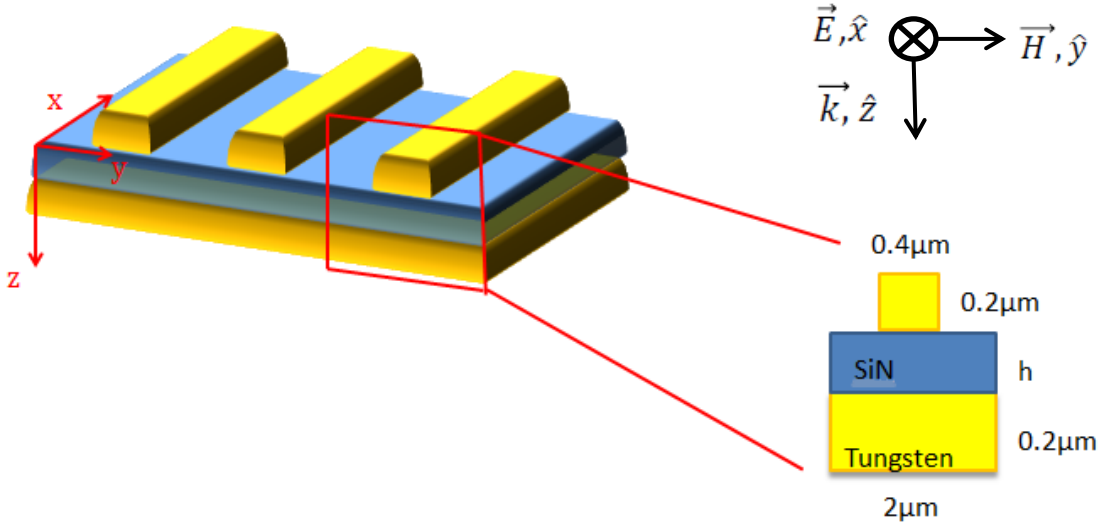

Figure 1. An incoming s-polarized (e.g. parallel to the x-direction) plane wave is incident to a metal dielectric-metal two dimensional periodic structure.

3.3 Definition of material Parameters

All parts of our structure are described by frequency dependent dielectric constants. They were calculated using standard methods and adjusted to the high temperatures. Unfortunately there is no data available for material parameters at higher temperatures so that these adjustments are estimates.

3.3.1 Metal (Tungsten)

For the description of the tungsten parts (back plate and wires/stripes) the frequency dependent Drude model has been used, with plasma frequency ω_p =1448THz and collision frequency ω_c=50THz [3]. The following relation is proved in the theoretical part (fig.2):

$$\epsilon(\omega) = 1 - \frac{\omega_p^2}{\omega(\omega + i\omega_c)}$$

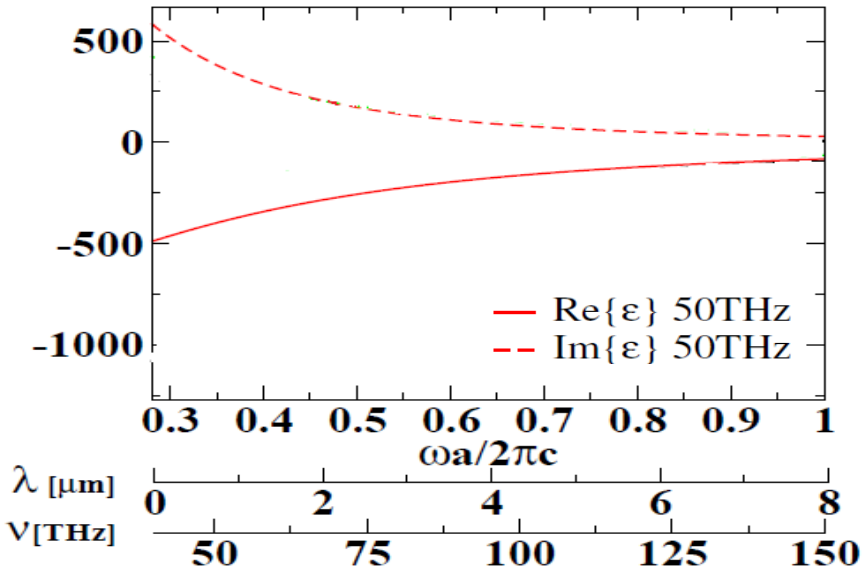

Figure 2. Drude dispersion relation for the metal back plate and wires.

The use of ω may be misleading however as used in standard bibliography we refer not to circular frequency but what physicists denote as f or ν measured in *Hz*.

3.3.2 Semiconductor Spacer (SiN)

The frequency dependent optical constants of Silicon Nitride were estimated using data in the range of 80-180nm [2]. This data has been extrapolated using Cauchy description for dielectrics (fig.3):

$$Re\{\mathrm{n}\} = \mathrm{A} + \frac{\mathrm{B}}{\lambda^2} + \frac{\mathrm{C}}{\lambda^4}, \quad Im\{\mathrm{n}\} = \mathrm{D} + \frac{\mathrm{E}}{\lambda} + \frac{\mathrm{F}}{\lambda^3}$$

leading to the following parameters:

A=2.16526 , B=20492, C=1

D= 0.00186 , E= - 16.53, F=$6.759 \cdot 10^6$

The frequency region we are interested in is (40-100) THz corresponds to (3000-7500) nm. We observe that in this THz regime the real part of the refractive index is 2.16526 and the imaginary part of the refractive index is 0.00186.

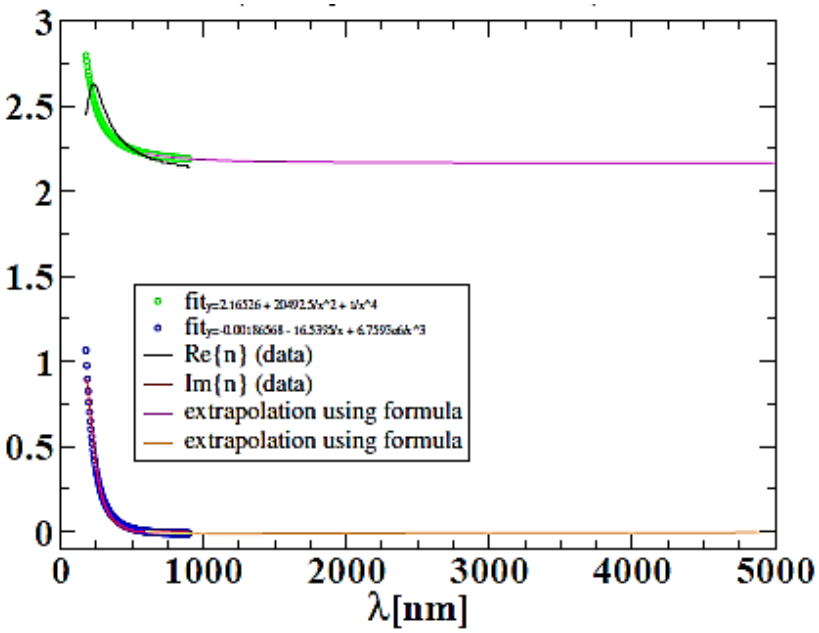

Figure 3. Index of refraction for Silicon Nitride. The strong dependence appears in the optical regime (250-600) nm. THz regime corresponds to a wavelength range approximately (3000-7500) nm.

3.3.3 Thermal adjustments

We suggest a modification to the imaginary part of dielectric permittivity due to thermal adjustments. We plot corresponding frequency dependent dielectric permittivity. The caption (upper right) depicts the variations due to higher temperatures (fig.4) :

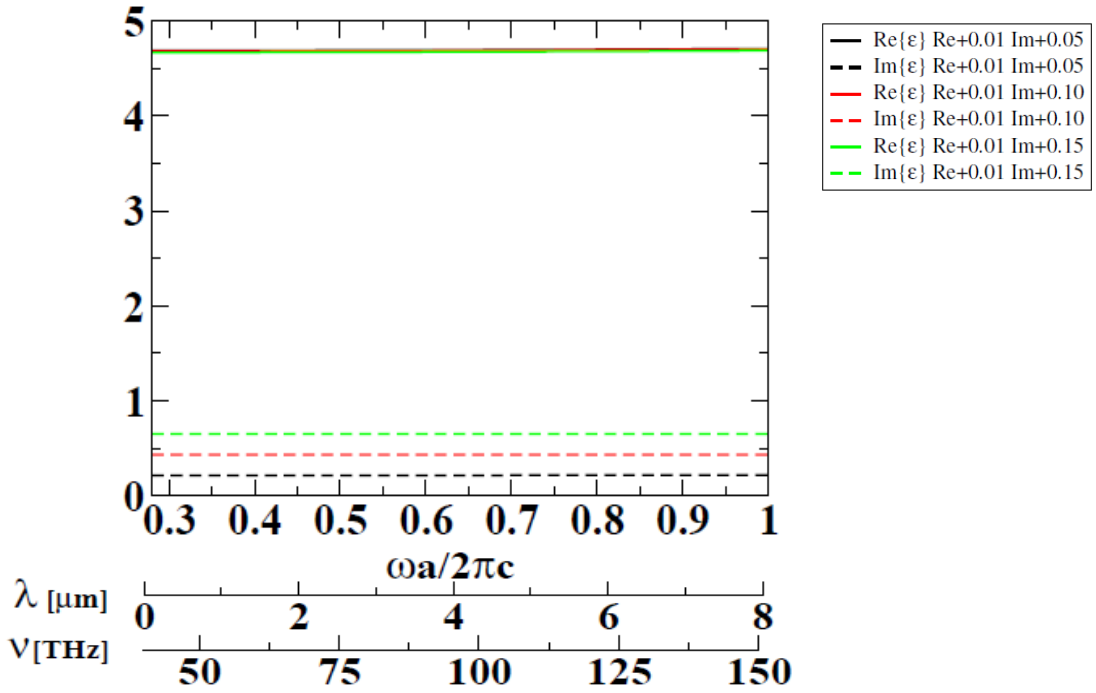

Figure 4. Frequency dependent dielectric permittivity

In our simulations we use $n = 2.16526$ for the real part of the refractive index and $k = 0.21$ for the imaginary part of the refractive index. In terms of complex dielectric permittivity that is $\hat{\varepsilon}$ = 4.69+0.42 i.

3.3.4 Optimum Absorbance

The careful reader would have noticed that the free parameter to be altered is the *height of the semiconductor h***.** We show that absorption tends to unity for a height of 0.5 μm at a resonance frequency $v_o = 87THz$ with a half-width at half-maximum ~40THz corresponding to 45.9% of the centre frequency. The broadband absorption is shown below (fig.5):

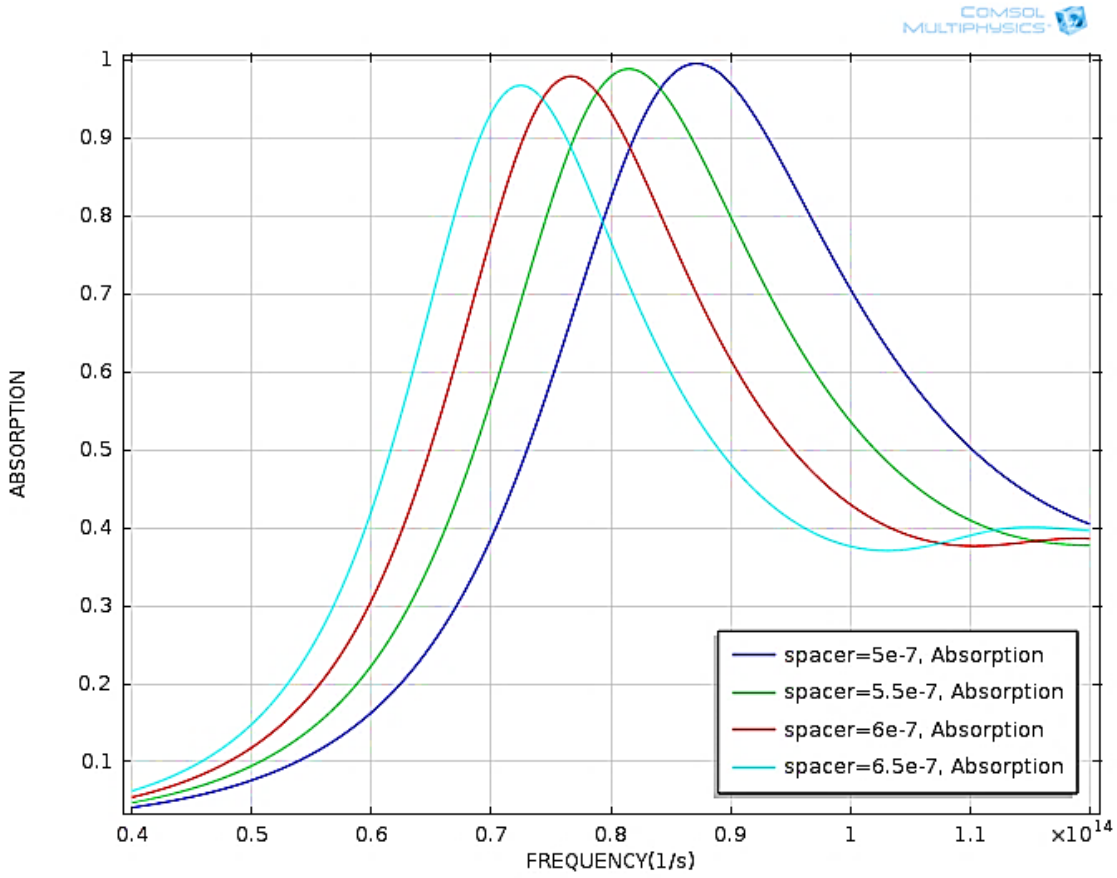

Figure 5. The decrease of semiconductor spacer from 0.65μm to 0.5μm results an increase to absorption that reaches 99.9 %.

We focus on the optimum absorption curve and present the full spectrum including not only absorption but transmission and reflection as well (fig.6):

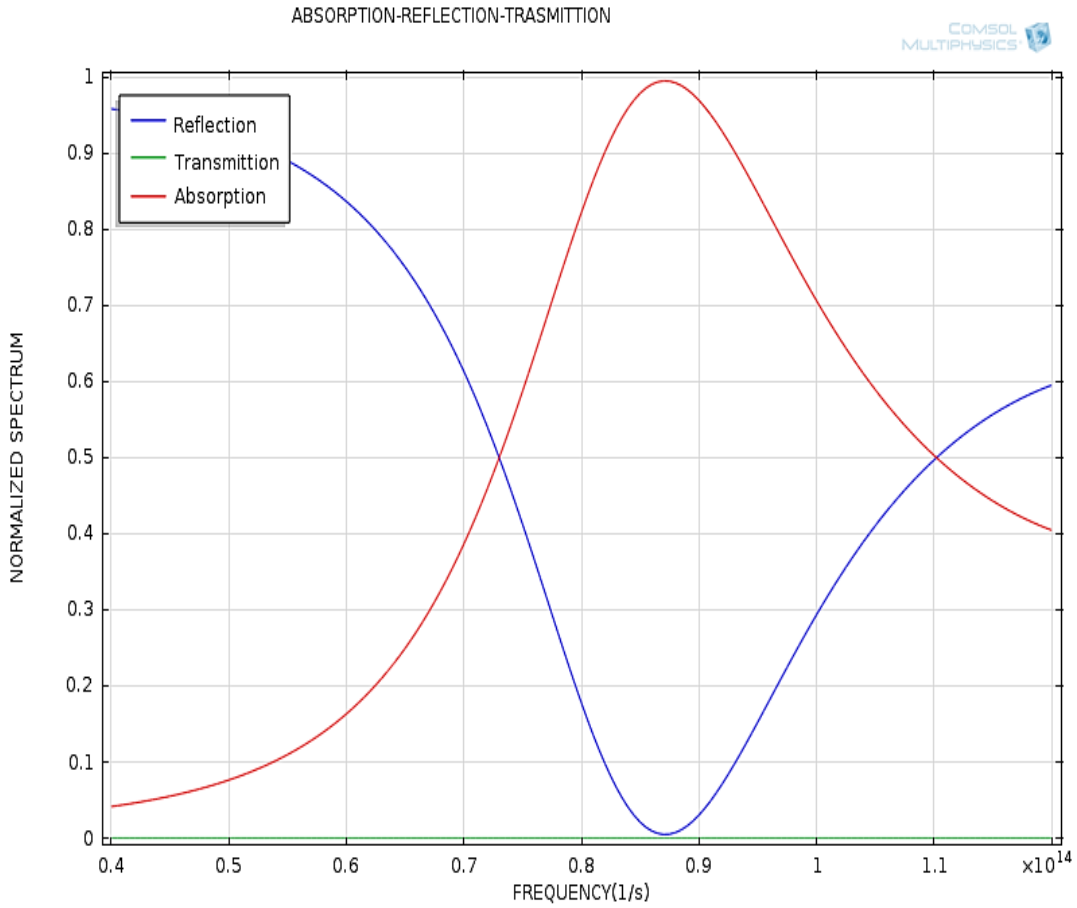

Figure 6. The metal back plate with a height of 0.2 μm that is much larger than the skin depth in THz regime avoids transmission through the structure.

We succeed zero reflection at resonance frequency by decreasing the dielectric height since we have ensured zero transmission from the back plate height.

3.3.5 Physical Mechanism

To get a physical intuition of the phenomenon, we plot the electromagnetic power loss density and the Poynting vector at resonance using the formulas (fig.7):

$$< P >= \frac{1}{2} \int_V \sigma(\omega) |\vec{E}| \, d^3r \ , \qquad \vec{P} = \vec{E} \times \vec{H}$$

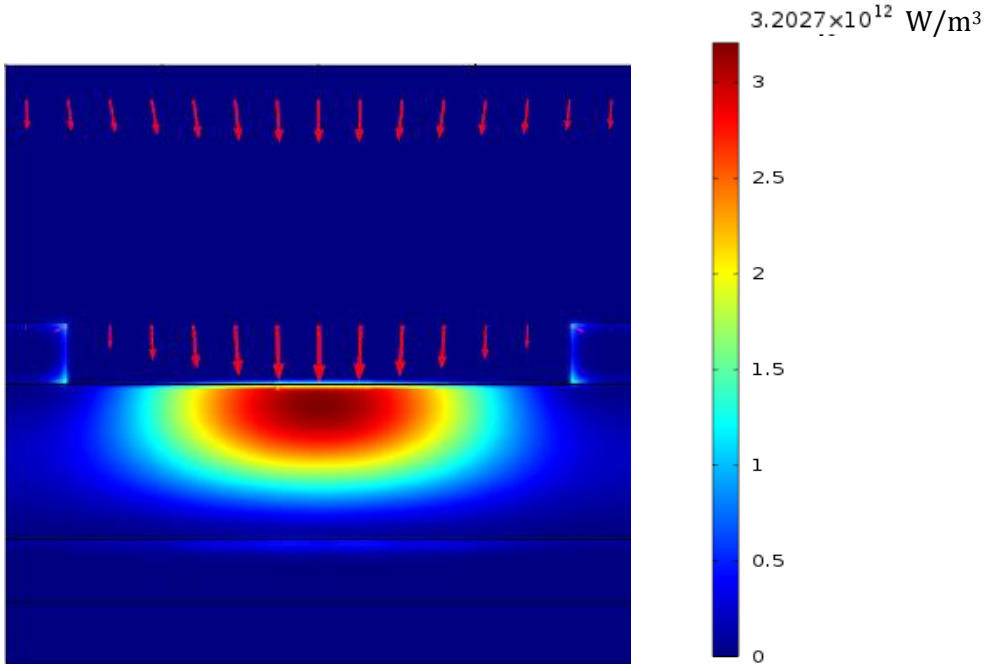

Figure 7. The surface plot depicts the electromagnetic power loss density (W/m^3) and the red arrows depict the power flow (W/m^2) described by the Poynting vector. The plots are at the resonance frequency of 87THz. The red color corresponds to a maximum of $3000MW/m^3$.

A strong enhancement of the losses is found at the region between metallic stripes within the semiconductor spacer. Therefore, the absorption is due to a sort of cavity formed that captures all incident radiation in the Silicon Nitride. The crucial part is the imaginary part of refractive index of SiN and the piles/stripes that capture the reflected radiation from the back plate. The height

of the back plate is 0.2μm. This is much larger than the typical skin depth in THz regime and avoids transmission through the structure. A rough estimation for tungsten skin depth assuming constant conductivity $\sigma = 1.8 \cdot 10^7 S/m$ at $20\,C^o$, $v = 50THz$ results δ=0.017μm which is much smaller than the proposed height. In this case the reflection is the only factor limiting the absorption. For completeness we would include plots of the absolute value of the z-component of the electric field E_z, the current density J_z, the magnetic field H_x and H_y at the resonance frequency of 87THz.

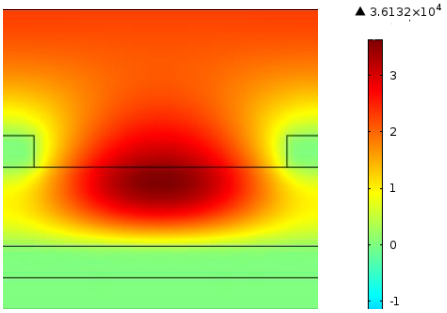

The z-component of electric field Ez.

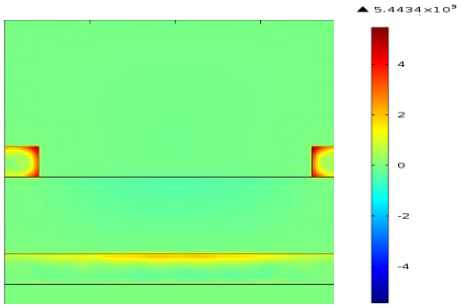

The z-component of current density Jz.

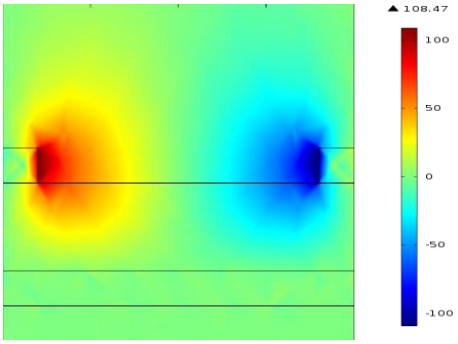

The y-component of magnetic field Hy.

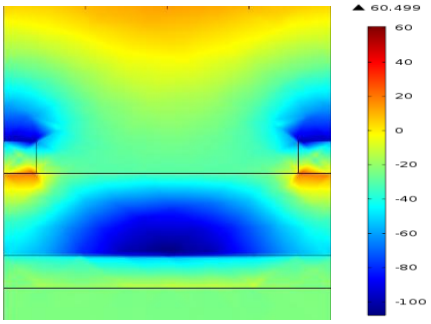

The x-component of magnetic field Hx.

The change in colors at the plot of J_z between dielectric and air (blue), and at the surface between back plate and dielectric (red) is a strong indication that antiparallel surface currents are driven [4],[5].

3.4 Scale down to reach the optical regime

We propose a diminish of the primary geometry with a scale factor 0.3 times the original dimensions and represent it schematically below (*fig. 8*):

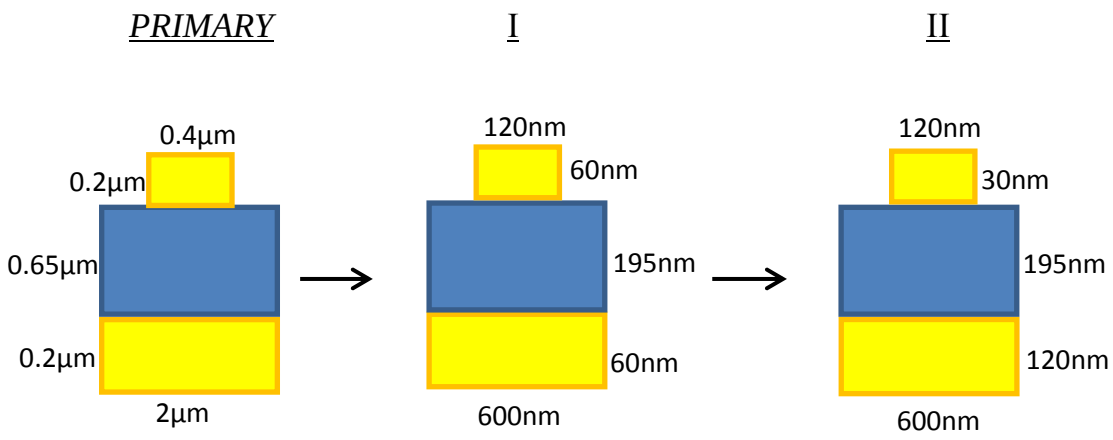

Figure 8. Demonstration of the 2 steps of geometry adjustments. First we multiply every dimension with 0.3 (I). Then, we shorten the pile height and increase the back plate (II).

In the first step, the results were not satisfying we succeed a 90% absorption and a 4% transmission. Therefore, we increased the back plate's height in order to get a zero transmission and decreased the pile's height to allow more incident radiation reach the semiconductor spacer. The result of the absorption/transmission/ reflection follows (fig. 9). The FWHM is 300THz and approaches 60.7% of the resonance frequency. This is a very broad frequency range at optical regime.

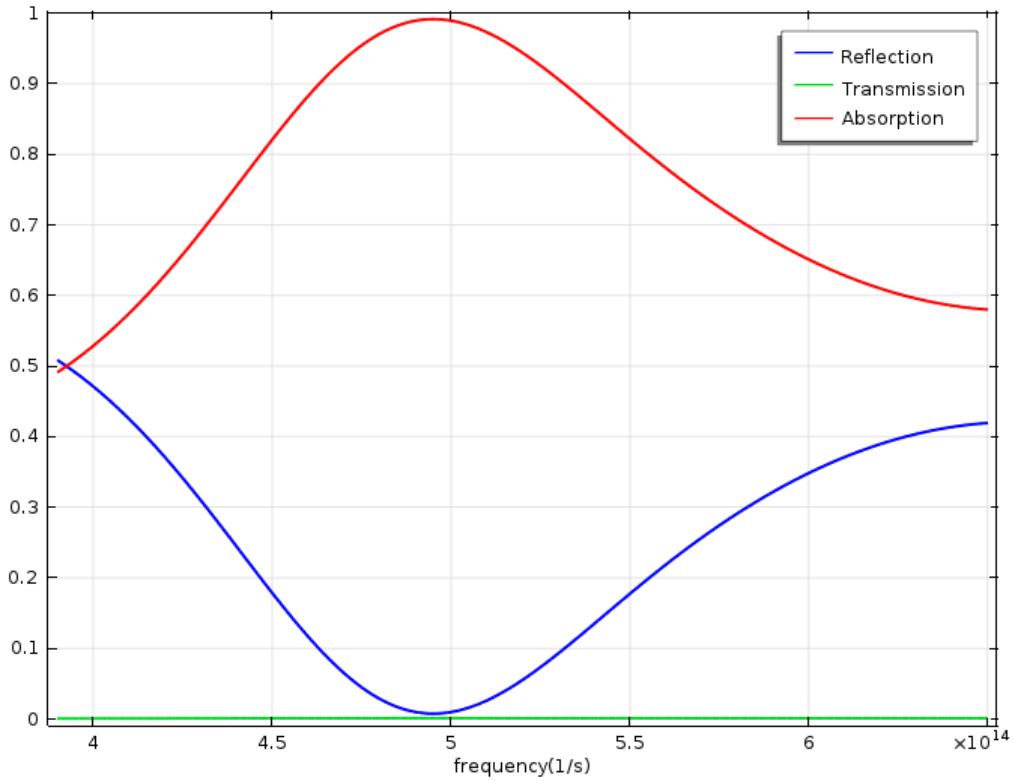

Figure 9. 99.9% absorption is achieved at a resonance frequency of $v_o = 494THz$ which corresponds to a wavelength λo=606nm.

We present the 3-D plot for the electromagnetic losses to underline the importance of the semiconductor spacer (fig.10):

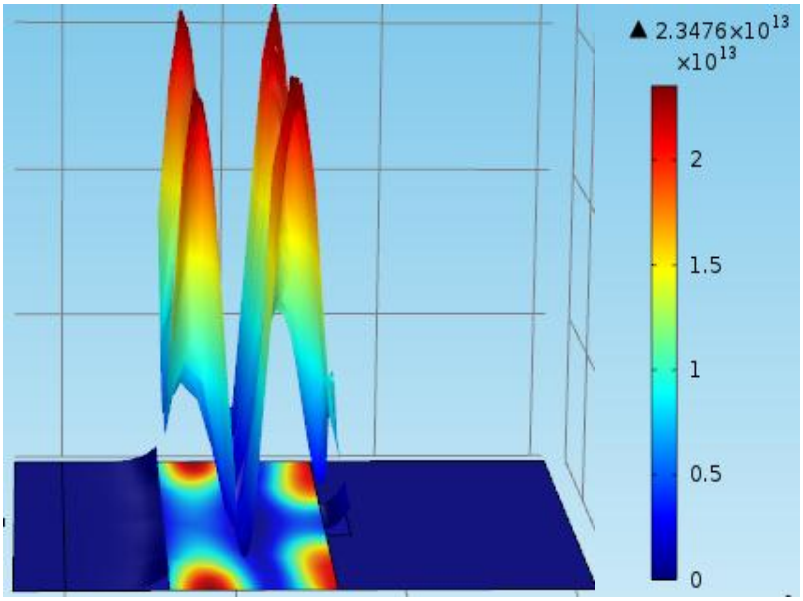

Figure 10. The 3-D plot of Electromagnetic losses. Structure is horizontally placed to show the strong enhancement within the dielectric. The values at the legend are measured in W/m^3.

For each part of our structure we seek the independent contribution to absorption to understand better their effect altogether. We observe almost zero contribution for the back plate , the pile, pile and the back plate (pink ,grey ,blue curve) each of them alone and all the other parts consist of air. Furthermore, the semiconductor spacer and the pile plus the spacer, each of them alone, share the same contribution to absorption namely 50%. A remarkable conclusion is that if the pile is taken away (red curve) the absorption is still near-unity [6].

On the other hand if the piles height is significantly increased absorption falls. What would be physically expected and it's not confirmed is that the contributions of back plate alone, and the semiconductor alone, and the pile alone, should result a near-unity absorption if the corresponding curves (pink plus green plus grey result the black) (Fig.11).

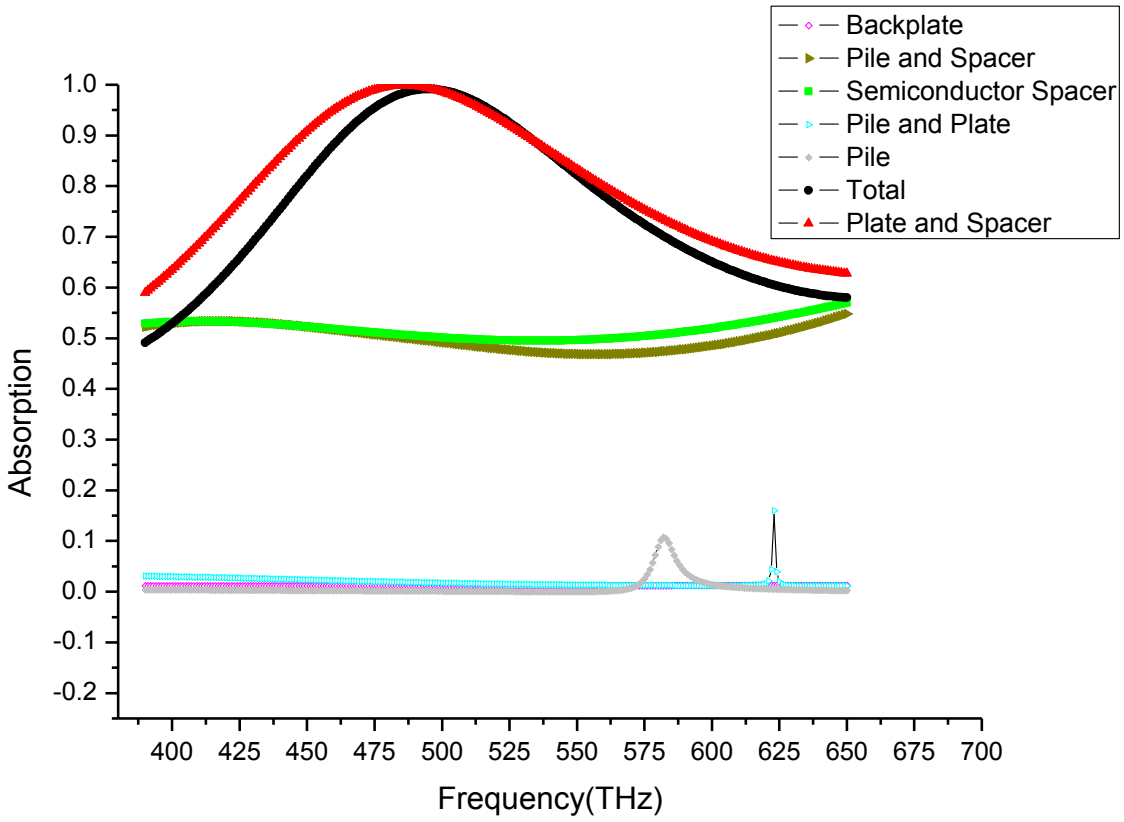

Figure 11. Absorption versus frequency for every possible combination of parts of the structure.

3.5 Oblique incidence at optical regime

If the structure is used as a perfect absorber, e.g., in sensor applications, it is important to absorb as much of the incident radiation as possible, independent of the direction of incidence. In Fig.12 we show the angular dispersion of the peak together with the spectra for several angles.

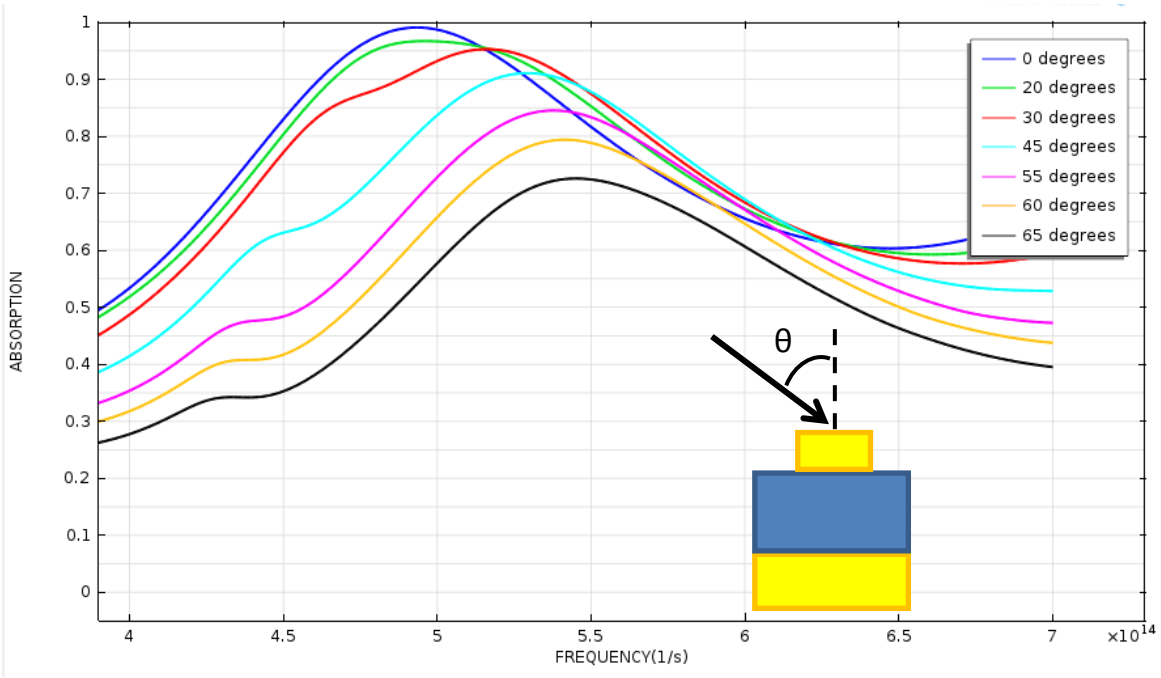

Figure 12. Angular dispersion of the absorption. For 0^0-45^0 the absorption is above 92%. Even at 65^0 still 73% of the incoming energy is absorbed.

For angles larger than 45^0 the resonant is blue-shifted to higher frequencies and an additional peak at lower frequencies are visible. Both peaks are caused by resonant modes in the dielectric as well, but their angular dependence shows a very strong dispersion.

References

[1] http://www.comsol.com/rf-module

[2] Phys. Rev. B 79, 033101 Marcus Diem, Thomas Koschny, and C. M. Soukoulis

[3] Applied Optics, Vol. 22, Issue 7, pp. 1099-1119 (1983) M. A. Ordal, L. L. Long, R. J. Bell, S. E. Bell, R. R. Bell, R. W. Alexander, Jr., and C. A. Ward

[4] Scientific Reports Nature 4, Article number: 4901 doi: 10.1038/srep04901

[5] Phys. Rev. Lett. 100, 207402 N. I. Landy, S. Sajuyigbe, J. J. Mock, D. R. Smith, and W. J. Padilla.

[6] Nature Communications 2, Article number: 517 doi:10.1038/ncomms1528 Koray Aydin, Vivian E. Ferry, Ryan M. Briggs & Harry A. Atwater.